Modeling and optimal control applying the flower pollination algorithm to doubly fed induction generators on a wind farm in a hot arid climate

Omar Chogueur[a], Saïd Bentouba[b], Mahmoud Bourouis[c*]

[a] University of Adrar, Laboratory of Sustainable Development and Computing (LDDI), 01000 Adar, Algeria

[b] Western Norway University of Applied Sciences, Faculty of Engineering and Science, Bergen, 5063, Norway

[c] Universitat Rovira i Virgili, Department of Mechanical Engineering, Av. Països Catalans No. 26, 43007 Tarragona, Spain

* Correponding Author: Email: mahmoud.bourouis@urv.cat

Abstract

In the present paper, the flower pollination algorithm (FPA) is employed for tuning the controller parameters of a Doubly Fed Induction Generator (DFIG) in a wind energy system. These parameters are then compared with those generated by the genetic algorithm (GA) and the proportional integral PI (initial design) controllers. Performance analysis of the DFIG is carried out in dynamic mode in two case studies. The first case study is carried out with no failure, the second one is subject to a short circuit in the electrical network. In this latter case study, a break occurs in the rotor circuit and disconnects the DFIG from the power grid. This gives rise to an excessive current in the rotor circuit which in turn influences the converters AC/DC/AC and makes the IGBT very sensitive. The genetic algorithm (GA) and the flower pollination algorithm (FPA) are used to tune the PI controllers with the purpose of improving the quality of a power supply should electrical disturbances occur.

The results show that by applying an optimal PI controller design to a Doubly Fed Induction Generator (DFIG) using the FPA the performance of the DFIG system can be improved in the event of disturbances. When the PI controller tuning using the genetic algorithm (GA) and the initial control system design is compared with the DFIG using the optimized design, a significant decrease in the overshoot of the rotor current and the DC-link voltage is observed.

Keywords: Doubly Fed Induction Generator, Wind farm, Genetic algorithm, Flower pollination.

Highlights

- A novel flower pollination algorithm (FPA) is developed for a DFIG-based wind power system.
- The overshoot rotor current and voltage of DFIG are significantly reduced when using the FPA-PI controller.
- The FPA-PI shows better control capacity than the GA-PI and PI initial design.
- The flower pollination algorithm is effectively used to solve technical faults on Kabaertan farm.

List of Abbreviations

ABC	Artificial Bee Colony Algorithm
AGC	Automatic generation Control
BESS	Battery Energy Storage System
DFIG	Doubly Fed Induction Generator System
FPA	Flower Pollination Algorithm
IGBT	Insulated-Gate Bipolar Transistor
GA	Genetic Algorithm
GSC	Grid Side Converter
MPPT	Maximum Power Tracking
PV	Photovoltaic
RSC	Rotor side converter
SMES	Superconducting Magnetic Energy Storage
VFC	Variable Frequency Converter
VSWT	Variable Speed Wind Turbine

List of Symbols

Latin symbols

C	Capacitance in DC link	[F]
F	Nominal frequency	[Hz]
H_g	Generator inertia constant	[s]
H_t	Turbine inertia	[KM^2]
I_d, I_q, I_α, I_β	2-axis currents	[A]
I_{gc}	Current through grid aside converter	[A]
I_{qgc_ref} , I_{dgc_ref}	2-axis currents references on grid side converter	[A]
I_r, I_s	Currents through rotor and stator	[A]
g_*	Actual best solution found among all solutions at the present iteration	[-]
Kp_{gc}, Ki_{gc}	GSC current regulator parameters	[-]

Kp_{rc}, Ki_{rc}	RSC current regulator gains	[-]
Kp_p, Ki_p	Power regulator parameters	[-]
Kp_V, Ki_V	Voltage regulator parameters	[-]
Kp_{Vdc}, Ki_{Vdc}	DC bus voltage regulator parameters	[-]
$L(\lambda)$	Levy flight-based step size	[-]
L_m	Mutual inductance	[H]
L_r	Self-inductance of rotor	[H]
P	Active power	[W]
P_{DC}	Instant active power into DC link	[W]
P_r	Active power of the rotor side converter	[W]
P_{ref}	Reference active power	[W]
Q	Reactive power	[VAR]
R_s	Resistance of the stator	[Ohm]
s	Slip of the rotor	[-]
S_n	Nominal apparent power	[VA]
t_e	Electromagnetic torque	[Nm]
t_m	Wind turbine torque	[Nm]
t_s	Shaft torque	[Nm]
t'_0	Time constant of rotor circuit	[-]
U'_q , U'_d	2-axis voltages transient reactance	[V]
V_a, V_b, V_c	3-phase voltages	[V]
V_d, V_q, V_α, V_β	2-axis voltages	[V]
V_{DC}	DC link capacitor voltage	[V]
$V_{DC_{ref}}$	Reference voltage of DC Link	[V]
V_{gc}	Grid side converter voltage	[V]
V_r	Terminal voltage of rotor	[V]
V_s	Terminal voltage of stator	[V]
V_{s_ref}	Terminal voltage of stator reference	[V]
x_i^t	Solution vector x of pollen i at iteration t	[-]
x_j^t and x_k^t	Solution vectors for pollen j and pollen k at iteration t	[-]

X_s	Reactance of the stator	[Ohm]
X_s'	Transient reactance of stator	[Ohm]
X_{Tgc}	Reactance of fed-back transformer	[Ohm]
$y_1, y_2, y_3, y_4, y_5, y_6, y_7$	Intermediate variables	[-]

Greek symbols

α	Pitch angle	[Deg]
α_{ref}	Reference pitch angle	[Deg]
Θ_s	Twist angle of shaft	[Rad]
γ	Scaling factor	[-]
ΔV	Voltage error when disturbance occurs	[V]
ΔP	Power error when disturbance occurs	[V]
ΔI_{rc}	Rotor current error when disturbance occurs	[V]
ΔI_{gc}	Grid current error when disturbance occurs	[V]
ΔV_{dc}	DC bus voltage error when disturbance occurs	[V]
$\lambda 1,\ \lambda 2,\ \lambda 3,\ \lambda 4,\ \lambda 5$	Selected weighting factors	[-]
φ	Angular position	[Rad]
$\Gamma(\lambda)$	Standard gamma function	[-]
Ω_s	Angular synchronous speed	[Rad]
Ω_t	Angular speed of turbine	[Rad]

1. Introduction

The use of renewable energies is inevitable to meet the growing demand for energy for all humanity. This is based on a real fear of climate change, depletion of fossil fuels and the instability of the oil market. Among the cleanest energy sources, wind power is one of the most popular renewable energy technologies for the following reasons. Wind power is actually the fastest growing energy source and is abundant in most parts of the world. It boasts low total air pollution, and no carbon dioxide emissions. Therefore, wind energy could be viewed as one of the best alternatives for use in generating electricity from renewable energy sources. Nevertheless, wind energy also presents some drawbacks, such as intermittency, variability and uncertainty, which are technological issues that need to be seriously addressed. In the power generation industry, wind power is among the most promising source for electricity generation. Indeed, today, of all the renewable energy sources, wind power is the world's fastest growing. The contribution of wind power to energy production is expected to reach 30% by 2050, and will correspond to an annual generation capacity of around 22 000 TWh [1].

It is widely reported in the literature that the variable-speed wind turbine (VSWT) with a doubly-fed induction generator (DFIG) is a promising system for wind power generation. It has the capacity to efficiently supply electrical energy. In this case, the stator of the induction generator is directly connected to the network, but the rotor terminal is connected to the transformer and the network through the AC/DC/AC variable frequency converter (VFC). It is worthy of note that the DFIG system offers several advantages. It is able to control the active and reactive power generator, produce energy expeditiously, improve power quality, and address dynamic disturbances such as voltage drop and short circuit issues. The VFC and IGBT switches encountered in DFIG systems are highly sensitive, particularly during transient disruptions in the network. The behaviour of the VFC converter is directly dependent on the performance of the DFIG system. In addition, the Rotor Side Converter (RSC) may get blocked when the VFC trip protects the DFIG rotor circuit from receiving excessive current. In such a case, the DFIG becomes independent of the power system. The electricity supply to consumers must be sufficient in quantity and of good quality. For this, a correctly designed controller is required in order to stabilize the power system and secure a reliable source of energy. Several investigations focused on advanced techniques applied in non-linear control of power systems are reported in the literature. Mahvash et al. [2], Makhloufi et al. [3] investigated the performances of three powerful metaheuristic algorithms, namely the cuckoo search algorithm (CSA), the firefly algorithm (FFA), and the flower pollination algorithm (FPA). The authors concluded that CSA algorithm was a suitable tool to optimize the Adrar power flow system in term of iterations and computational time. Ahmed et al. [4] reported on the importance of optimizing the gain and time constants in a lead-and-lag controller using three optimization algorithms: the particle swarm optimization (PSO) algorithm, the genetic algorithm (GA), and the flower pollination algorithm (FPA) [4]. The results showed that the FPA algorithm showed the highest appropriate value [(-2.3725×10^6)] as the GA algorithm showed a value of [(−2.3813 x 10^6)] and the PSO algorithm [(−2.3796 x 10^6)]. Non-linear time domain simulation and quantitative analysis showed that the FPA algorithm was better in optimizing the control parameters for a lead-lag controller in a DFIG-based wind power system. Qu et al. [5] investigated the potential application of a novel multi-objective optimization algorithm to optimize the forecasting approach of wind-speed. In this case, a new hybrid flower pollination algorithm and a bat search algorithm were proposed to search for the optimal weight coefficients. Abdelaziz et al. [6] used the FPA algorithm to solve the economic load dispatch (ELD) and combined economic emission dispatch (CEED) problems encountered in electrical power systems. The results obtained with the FPA algorithm proposed, were then compared with those of other optimization algorithms used for various power systems. The authors concluded that the FPA proposed outlasts other techniques, even in the case of large scale power systems, in terms of total cost and computational time with respect to valve point effects. The control techniques taken into consideration, have a complex structure and a higher stability. The PI controller is the most popular controller used in control techniques for power systems and is used in wind turbines because of its simple structure [7]. It is worthy of note that tuning PI controllers in highly complex nonlinear systems is very complicated and hard to achieve, however, this may be overcome by applying intelligent computing to determine the PI controller parameters. A large variety of algorithms were applied in different power generation systems to determine the optimal value of a system . Indeed, the computational method called the PSO algorithm, was employed in tuning and optimizing the parameters of a PI controller on a doubly fed induction generator (DFIG) system [8]. The CSA algorithm was used for tuning the PID controller parameters in a self-excited induction generator (SEIG) [9], and the ABC algorithm was employed in a multi-area power system with multiple interconnected generators [10]. The Differential Evolution (DE) algorithm was used for tuning the PI controller parameters on a doubly fed induction generator (DFIG) [11].

Among the different types of algorithms developed, the population-based search algorithm, which uses recombination and selection methods to obtain the optimum parameter value of the PI controller, is of great interest for the application investigated in the present paper. This approach, introduced initially by Yang et al. [12] in 2013, was called the flower pollination algorithm (FPA). The authors reported in depth on the main challenges associated with these metaheuristic algorithms. The FPA algorithm was widely used in recent investigations and showed promising results. It was applied in the load frequency control of multi-area interconnected power systems with nonlinearities [13] to optimize the PID controller for Wind-PV-SMES-BESS-Diesel Autonomous Hybrid Power Systems [14]. The FPA algorithm was also employed for the optimization of controllers in a DFIG system. In the present work, the flower pollination algorithm (FPA) is used for the first time to establish the optimal parameters of multiple PI controllers on a rotor side converter (RSC) of a DFIG system to improve system performance when a failure or interruption occurs. The performance of an optimized PI controller is assessed using the Integral Time Absolute Error (ITAE). A number of simulations were performed at normal working conditions and at fault conditions in order to test the performance of the control system in both circumstances. Afterwards, the results of the simulations carried out with the PI initial design controller were compared with those obtained with the PI-based GA controller and the PI-based FPA controller, and reported by Hanan et al. [15] and Zemmit et al. [16].

Mohammadi et al. [17] carried out a performance evaluation of wind turbines (WTs) during faults to check system stability, protection, and lifetime. The effects of short circuit faults on the electrical and mechanical parts of fixed-speed WTs were investigated. The authors reported that short circuit faults not only have severe effects on the electrical parts of the WTs, but that they can also generate vibrations on the mechanical parts such as the blades and the tower that can reduce their lifetime.

In this paper, the flower pollination algorithm (FPA) is used for tuning the controller parameters of a Doubly Fed Induction Generator (DFIG) on wind farms. The investigation is carried out in dynamic mode in two case studies. The first case study not subject to a failure, but the second one undergoes a short circuit in the electrical network. In this latter case study, a break occurs in the rotor circuit and disconnects the DFIG from the power grid. This gives rise to an excessive current in the rotor circuit that influences the converters AC/DC/AC and makes the IGBT very sensitive. The approach developed is applied in a real case study, namely the Kabertan wind farm located in the south of Algeria.

2. Description of the Kabertan wind farm

The wind farm used in the present paper is located near a Sonelgaz electrical post in Kabertan, located 73 km north of the city of Adrar in southwestern Algeria. The altitude of the site is 260 m and its geographical coordinates are Latitude: 28°27'7.44”N and Longitude: 0°02'59.08”W. The decisive factor in the choice of a site for wind farms is the wind speed. In Kabertan, an average wind speed of 6, 62 m/s was recorded for the period of 2008-2013. The wind farm installed in Kabertan was the first important installation for wind power generation in Algeria. It consists of 12 wind turbines with doubly fed induction generators supplied by the manufacturer Gamesa. The nominal power production of the wind farm is 10.2 MW with an annual production of 27 GW/h. Table 1 summarizes the main specifications of the wind farm.

Table 1. Main specifications of the Kabertan wind turbine.

Designation	**Characteristic**
Wind turbines	12 type Gamesa G52
Blades Turbine	3/26 m long
Mast height	55 m
Power Unit	850 kW
Energy evacuation	Kabertene 30/220 kV substation
Annual energy produced	27 GWh
CO_2 avoided / year	5800 tonnes

3. Algorithms and methodology

3.1. Modeling of wind farm and Systems

Wind power generation refers to the technology that employs wind turbines to convert the wind's kinetic energy into electric power. The system used in this study is a doubly fed induction generator (DFIG) wind turbine used on the Kabertan wind farm. The wind farm production is connected to the 30/220 kV Kabertan Injector via two underground cables which link the substation with MV distribution cells of 30 kV. The cells use the transformer distribution system to export the power to a 220 kV network, as shown in Figure 1.

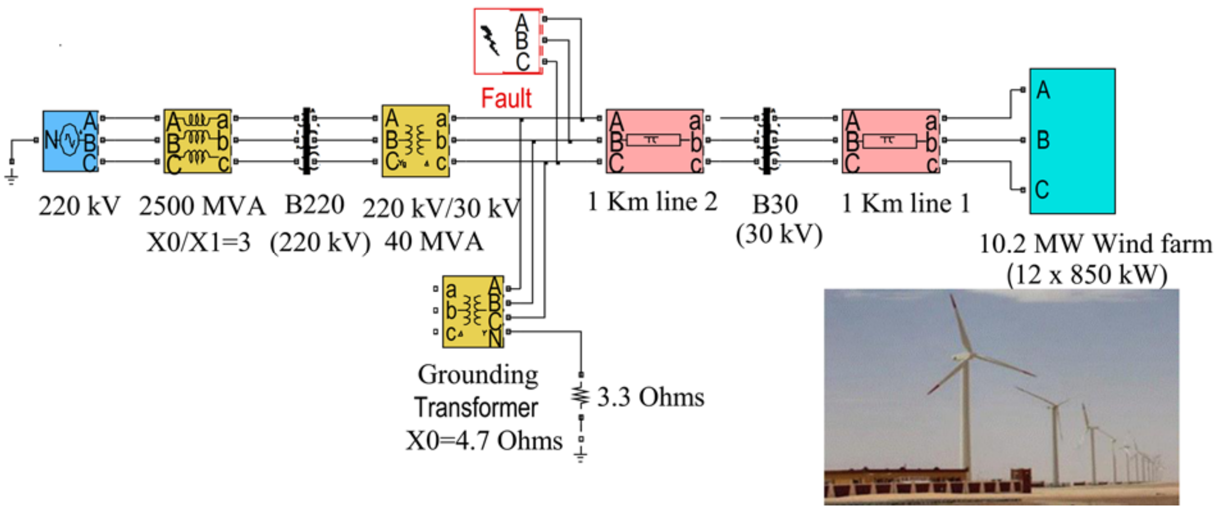

Figure 1. Scheme of the 10.2 MW wind farm connected to the distribution network.

The wind farm in question consists of 12 doubly fed induction generator (DFIG) based wind turbines. Each wind turbine has a power output of 850 kW with a nominal voltage of 690 V. Table 2 summarizes the data parameters of the wind turbine DFIG.

Table 2. WT-DFIG data parameters.

WT-DFIG Data	
Nominal power P (KW)	850
voltage U (V)	690
Nominal apparent power S_n (KVA)	890
frequency F (Hz)	50
pair of poles	2
Stator resistance R_s (Ohm)	0.0033
Stator leakage reactance L_s (H)	0.0064
Rotor resistance R_s (Ohm)	0.0028
self-inductance of rotor L_r (H)	0.0065
mutual inductance L_m (H)	0.0064
Generator inertia Constant H_g(s)	5.04
Turbine inertia H_t	4.17
Nominal DC voltage (V)	1200
DC-link capacitance C (F)	0.06
Pitch controller gain	120
Pitch angle (Deg)	-5° to 90°

The Kabertan wind farm has been exploited since July 2014. This wind farm suffers certain technical problems like short circuit faults. The present paper considers the configuration of the Kabertan wind farm in order to propose technical solutions to these problems. Figure 2 shows the electrical layout of this wind farm. The wind turbines consist of a DFIG generator from a wound rotor induction generator and a PWM conversion based on IGBT-AC/DC/AC.

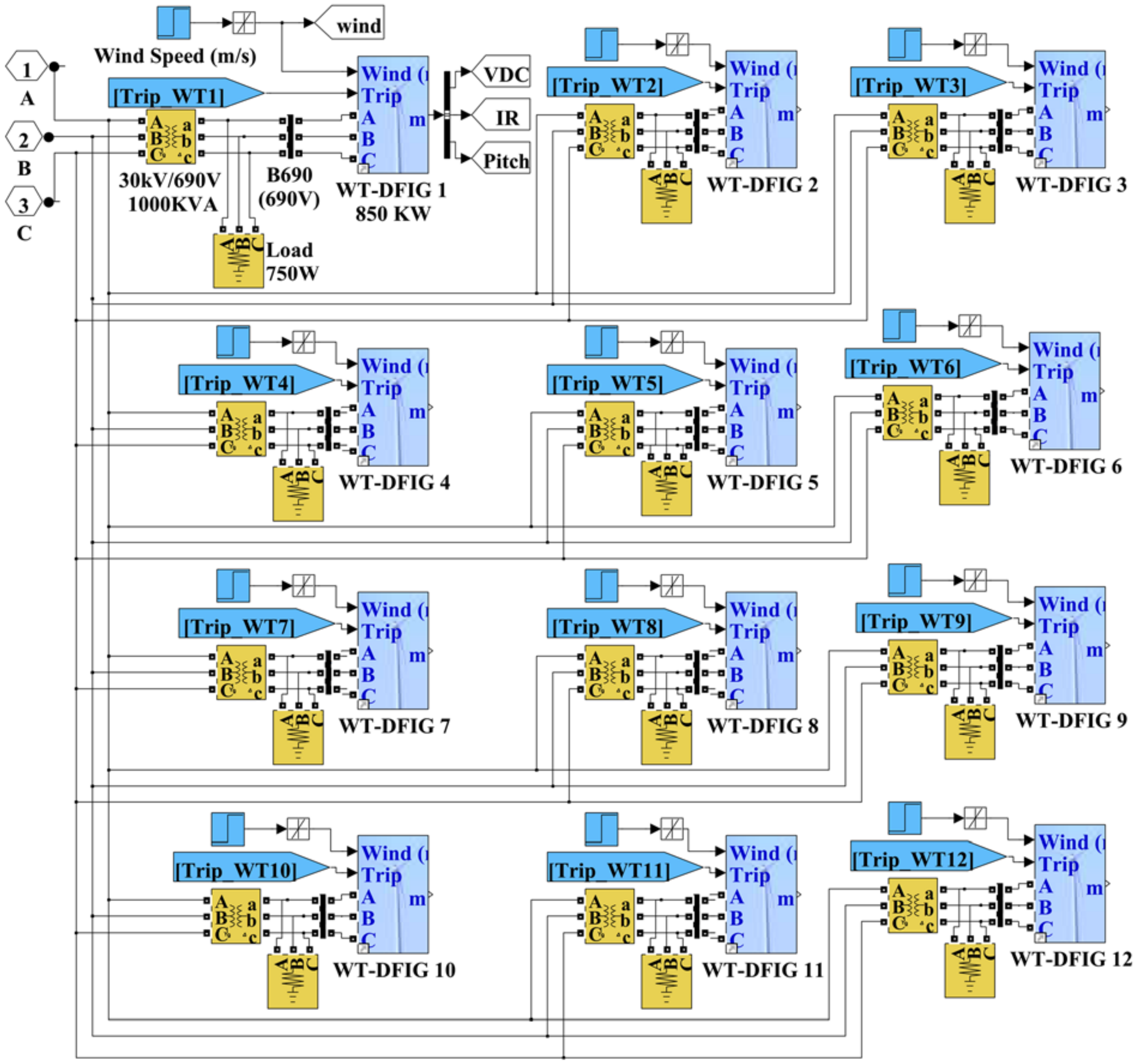

Figure 2. Electrical layout of the Kaberten wind farm (12×850 kW).

3.2. Wind Energy conversion

The AC/DC/AC converter includes two essential components, namely the rotor-side converter (RSC) and the grid-side converter (GSC). These two components are Voltage-Sourced Converters using forced-commutated power electronic devices, such as the Insulated-Gate Bipolar Transistors (IGBTs), and generate an AC voltage from a DC voltage (VDC) generator. A capacitor connected to the DC part operates as the DC voltage (VDC) source. In addition, the GSC is connected to the grid by means of a coupling inductor L. Similarly, the stator of the induction generator is directly connected to the grid (network), but the rotor terminal is connected to the network through the AC/DC/AC variable frequency converter (VFC). The power caught by the wind turbine is converted by the induction generator into electrical power, which is then transmitted to the grid through the windings of the stator and rotor. The control system supplies the blade pitch angle command, the voltage command signals

Vr and Vgc for RSC and GSC respectively in order to control the power of the wind turbine, the DC bus voltage and the voltage at the grid terminals, as shown in Figure 3.

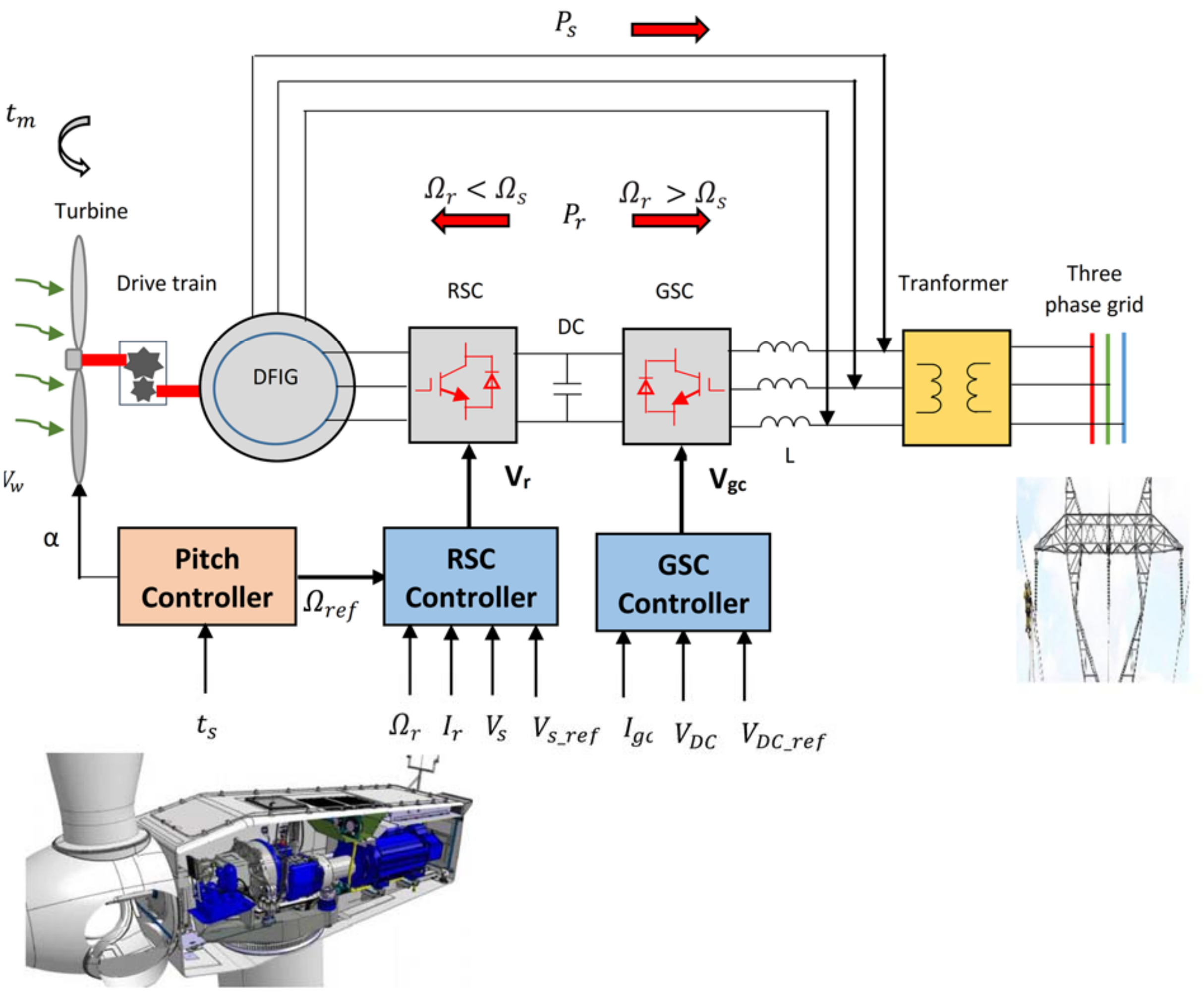

Figure 3. Wind turbine with the doubly fed induction generator system.

3.2.1 Modeling of drive train

The mechanism of the two-mass drivetrain model is considered. The differential equations describing the dynamics of the system may be expressed as:

$$\frac{d\Omega_t}{dt} = \frac{1}{2H_t}(t_m - t_s) \tag{1}$$

$$\frac{d\Theta_s}{dt} = \Omega_t - (1 - s)\Omega_s \tag{2}$$

$$\frac{ds}{dt} = \frac{-1}{2H_g\Omega_s}(t_e + t_s) \tag{3}$$

Where;

Ω_s is angular synchronous speed, Ω_t is angular speed of turbine, H_t is turbine inertia, t_s is shaft torque, t_m is wind turbine torque, H_g is generator inertia, Θ_s is twist angle of shaft, s is slip of the rotor, t_e is electromagnetic torque.

3.2.2 Modeling of pitch control

The pitch angle of the turbine is adjusted, at high wind speeds, by the pitch controller for the purpose of controlling the power [18]. The pitch angle reference is set to zero when the wind speed values are less than the rated wind speed. Figure 4 depicts the pitch controller block diagram.

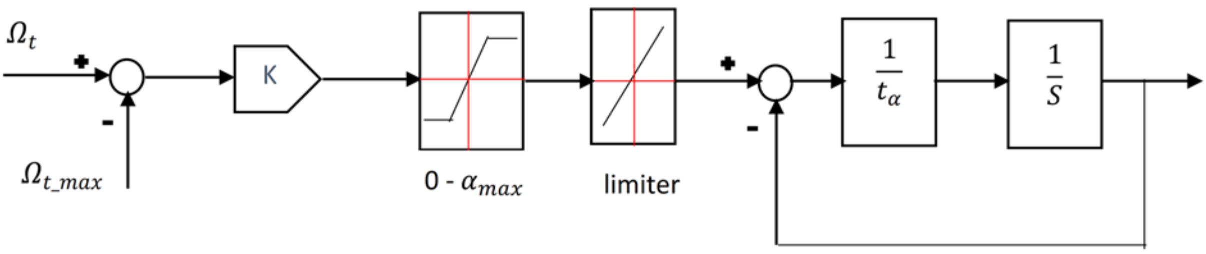

Figure 4. Block diagram of pitch controller.

Equation (4) is used to model the pitch control:

$$\frac{d\alpha}{dt} = \frac{1}{t_\alpha}(\alpha_{ref} - \alpha) \qquad (4)$$

Where;

α_{ref} is the reference pitch angle, α is pitch angle

3.2.3 Modeling of doubly fed induction generator (DFIG)

Equations (5 - 14) are the dynamic equations that represent the induction generator in the *d–q* reference frame.

<u>Stationary abc reference to stationary ***αβ***:</u>

Voltages:

$$V_\alpha = \sqrt{3}V_{ab} + \sqrt{3}/_2 V_{bc} \qquad (5)$$

$$V_\beta = 3/_2 V_{bc} \qquad (6)$$

Currents:

$$I_\alpha = {}^{3}/_{2}\, I_a, \tag{7}$$

$$I_\beta = {}^{\sqrt{3}}/_{2}\, V_{bc}(I_b - I_c) \tag{8}$$

<u>Stationary *αβ* reference to rotating *dq*:</u>

Voltages and currents:

$$V_d = V_\alpha cos\varphi - V_\beta sin\varphi \tag{9}$$

$$V_q = V_\beta cos\varphi - V_\alpha sin\varphi \tag{10}$$

where φ is the angular position of the *dq* reference frame.

In order to have the same amplitude as the phase quantities, the *dq* variables are scaled as follows:

<u>Delta connection</u>

$$V_d = \frac{2V_d}{3\sqrt{2}}, \qquad V_q = \frac{2V_q}{3\sqrt{2}}, \qquad I_d = \frac{2I_d}{3\sqrt{6}}, \qquad I_q = \frac{2I_q}{3\sqrt{6}}$$

<u>Star connection</u>

$$V_d = \frac{2V_d}{3\sqrt{6}}, \qquad V_q = \frac{2V_q}{3\sqrt{6}}, \qquad I_d = \frac{2I_d}{3\sqrt{2}}, \qquad I_q = \frac{2I_q}{3\sqrt{2}}$$

$$\frac{dU_d^{'}}{dt} = s\Omega_s U_q^{'} - \Omega_s \frac{L_m}{L_r} V_{qr} - \frac{1}{t_0^{'}}\left[U_d^{'} + \left(X_s - X_s^{'}\right) I_{qs}\right] \tag{11}$$

$$\frac{dU_q^{'}}{dt} = -s\Omega_s U_d^{'} - \Omega_s \frac{L_m}{L_r} V_{dr} - \frac{1}{t_0^{'}}\left[U_q^{'} + \left(X_s - X_s^{'}\right) I_{ds}\right] \tag{12}$$

$$\frac{dI_{ds}}{dt} = \frac{\Omega_s}{X_s'}\left[V_{ds} - \left(R_s + \frac{1}{\Omega_s t_0'}(X_s - X_s')\right) I_{ds} - (1-s)U_q^{'} - \Omega_s \frac{L_m}{L_r} V_{dr}\right]$$

$$+ \ \frac{1}{X_s' t_0'} U_q' + \ \Omega_s I_{qs} \tag{13}$$

$$\frac{dI_{qs}}{dt} = \frac{\Omega_s}{X_s^{'}}\left[V_{qs} - \left(R_s + \frac{1}{\Omega_s t_0^{'}}\left(X_s - X_s^{'}\right)\right) i_{qs} - (1-s)U_d^{'} - \Omega_s \frac{L_m}{L_r} V_{qr}\right]$$

$$- \ \frac{1}{X_s' t_0'} U_d' - \ \Omega_s I_{ds} \tag{14}$$

where;

U_q' is the voltage transient reactance on *q*-axis, U_d' the voltage transient reactance on *d*-axis, L_r the rotor self-inductance, i_s is the current through stator, t_0' the time constant of the rotor circuit, L_m the mutual inductance, V_r the rotor terminal voltage, V_s is the stator terminal voltage, R_s the stator resistance, $X_s^{'}$ is the transient reactance of stator, $X_s^{'}$ the stator transient reactance, and X_s the stator reactance.

3.2.4 Modeling of rotor side converter (RSC)

Figure 5 explicitly shows that the aim of the rotor side converter (*RSC*) is to regulate the terminal voltage (V_s) and output active power (P) by using I_{qr} and I_{dr} currents. The active power and terminal voltage can be controlled by means of nested PI controllers using intermediate variables. Then, the active power reference P_{ref} is obtained using a technique of maximum power tracking [19-21] and then compared with the actual value. The resulting error is then sent to the PI controller, which produces the reference current I_{dr_ref}. Likewise, the reference current I_{qr_ref} is generated following a similar procedure.

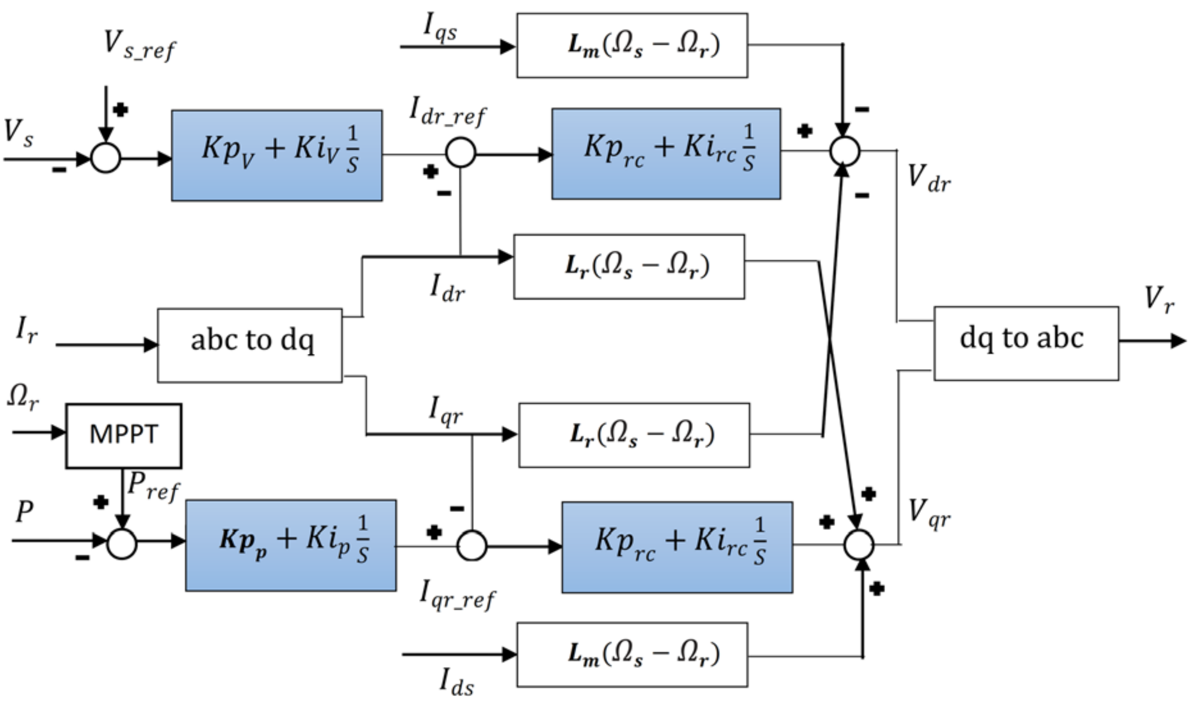

Figure 5. Rotor side converter control system.

Figure 5 illustrates the control mechanism of the rotor side controller. Subsequently, the current mentioned above are compared with actual currents, and the resulting errors are sent to the PI controllers.

$$\frac{dy_1}{dt} = V_{s\_ref} - V_s \quad (15)$$

$$\frac{dy_2}{dt} = Kp_V(V_{s\_ref} - V_s) + Ki_V y_1 - I_{dr} \quad (16)$$

$$V_{dr} = Kp_{rc}\left(Kp_V\left(V_{s_{ref}} - V_s\right) + Ki_V y_1 - I_{dr}\right) + Ki_{rc} y_2 \quad - (I_{qs}L_m + I_{dr}L_r)(\Omega_s - \Omega_r) \quad (17)$$

$$\frac{dy_3}{dt} = P_{ref} - P \quad (18)$$

$$\frac{dy_4}{dt} = Kp_p(P_{ref} - P) + Ki_p y_3 - I_{qr} \quad (19)$$

$$V_{qr} = Kp_{rc}\left(Kp_p(P_{ref} - P) + Ki_p y_3 - I_{qr}\right) + Ki_{rc} y_4 + I_{ds}L_m$$

$$+I_{qr}L_r)(\Omega_s - \Omega_r) \quad (20)$$

Where;

.y_1, y_2, y_3, y_4 are intermediate variables, Kp_p, Ki_p are the power regulator parameters, Kp_{rc}, Ki_{rc} are RSC current regulator gains, Kp_V, Ki_V are voltage regulator parameters, I_r is the current through rotor, I_s the current through stator, P the active power, P_{ref} the reference active power, and V_s is the ac terminal voltage, V_{s_ref} is the ac terminal voltage reference.

3.2.5 Modeling of the DC link

The active power of the Rotor side converter is the Grid side converter + the DC link capacitor. The governing equations are as follows:

$$P_R = P_g + P_{DC} \quad (21)$$

$$P_g = V_{dgc}I_{dgc} + V_{qgc}I_{qgc} \quad (22)$$

$$P_r = V_{qr}I_{qr} + V_{dr}I_{dr} \quad (23)$$

$$P_{DC} = V_{DC}I_{DC} = -CV_{DC}\frac{dV_{DC}}{dt} \quad (24)$$

$$CV_{DC}\frac{dV_{DC}}{dt} = V_{dgc}I_{dgc} + V_{qgc}I_{qgc} - \left(V_{qr}I_{qr} + V_{dr}I_{dr}\right) \quad (25)$$

$$V_{dgc} = Kp_{gc}\left(-Kp_{Vdc}\left(V_{DC_{ref}} - V_{DC}\right) + Ki_{Vdc} y_5 - I_{dgc}\right) + Ki_{gc} y_6 + X_{Tgc}I_{dgc}$$

$$+V_{ds} \quad (26)$$

$$V_{qgc} = Kp_{gc}\left(I_{qgc_{ref}} - I_{qgc}\right) + Ki_{gc} y_7 + X_{Tgc}I_{dgc} + V_{qs} \quad (27)$$

Where;

V_{gc} is the grid side converter voltage, V_{DC} the DC link capacitor voltage, I_{qgc_ref} is reference of q-axis on the grid side converter, I_{gc} the current through the grid side converter, P_{DC} is the instant active power into the DC link, P_r the active power of the rotor side converter, X_{Tgc} is the reactance of fed-back transformer, and C is the capacitance in the DC link.

3.2.6 Modeling of the grid side converter (GSC)

As illustrated in Figure 6, the grid side converter (*GSC*) is used for regulating the reactive power and for controlling the DC link voltage (V_{DC}) through the use of *i*qg and *i*dg currents. It should be emphasized that it is possible to control the reactive power and the DC link voltage using two series of PI controllers with intermediate variables. Moreover, Figure 6 displays the control mechanism of the grid side converter.

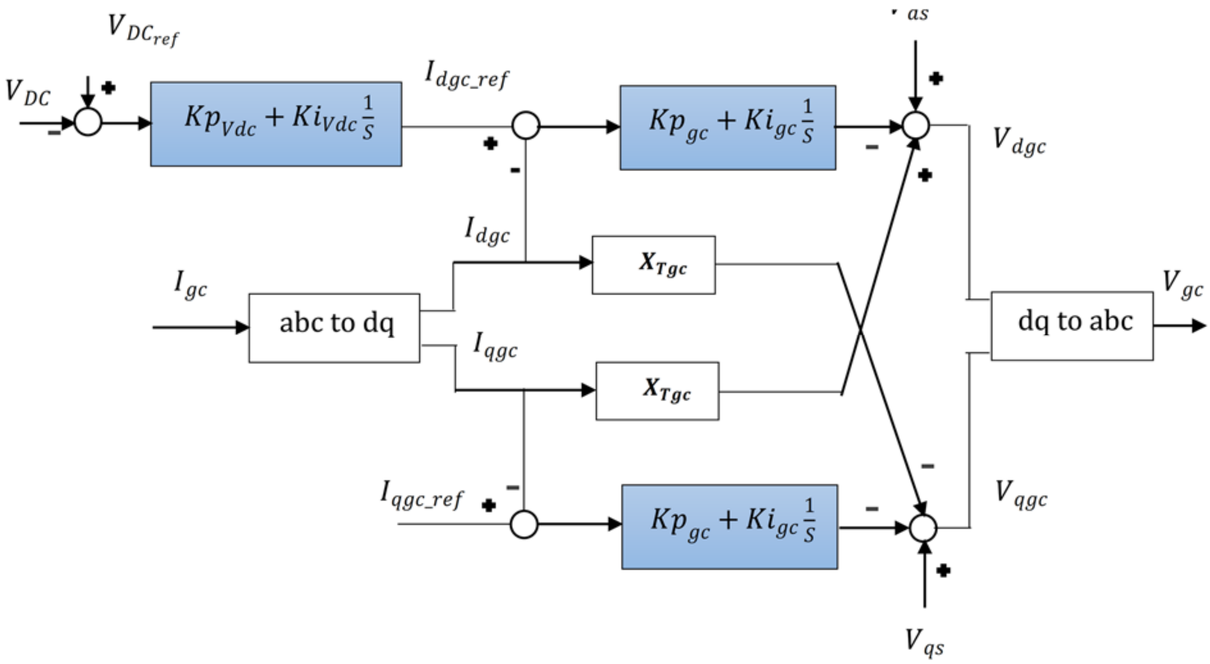

Figure 6. Grid side converter control system.

The GSC controller is governed by Equations (28–30);

$$\frac{dy_5}{dt} = V_{DC_{ref}} - V_{DC} \tag{28}$$

$$\frac{dy_6}{dt} = -Kp_{dc}\left(V_{DC_{ref}} - V_{DC}\right) + Ki_{dc}y_5 - I_{dgc} \tag{29}$$

$$\frac{dy_7}{dt} = I_{qgc\_ref} - I_{qgc} \tag{30}$$

Where;

y_5, y_6, y_7 are the intermediate variables, Kp_{Vdc}, Ki_{Vdc} are the DC bus voltage regulator parameters, Kp_{gc}, Ki_{gc} are the GSC current regulator parameters, and $V_{DC_{ref}}$ is the reference voltage of the DC Link.

4. Optimum design of a PI controller using the flower pollination algorithm

In this study, the flower pollination algorithm (FPA) is applied to the DFIG in order to automatically determine the optimal parameters of PI controllers on a rotor side converter (RSC) in a DFIG system. In the RSC regulation loop, there are five PI controllers; and each controller has two tuning values which are the controller gain and the integral time constant. The main purpose of using an FPA algorithm is to determine the optimal parameters of the three PI controllers present in the RSC settings. These are the PI controller proportional gains of the AC-bus voltage regulator, the power regulator, and the current regulator (Kp_V, Kp_p, Kp_{rc}), in addition to the integral time constants (Ki_V , Ki_p, Ki_{rc}). In order to control the grid-side converter (GSC) regulation loop response, the two PI controllers on the rotor side converter (RSC) in the DFIG system are tuned in accordance with the PI parameters, i.e. the current regulator (Ki_{gc}, Ki_{gc}) and the DC Voltage regulator (Kp_{Vdc}, Ki_{Vdc}) and using the flower pollination algorithm (FPA). Therefore each vector of the FPA has ten controller parameters as expressed by equation (25):

$$X = \left[Kp_V\ , Ki_V\ , Kp_p, Ki_p\ , Kp_{rc}\ , Ki_{rc}\ , Kp_{gc}\ , Ki_{gc}\ , Kp_{Vdc}\ , Ki_{Vdc}\ \right] \qquad (25)$$

The PI controller performance of the system investigated can be measured in the time domain by considering several parameters such as the overshoot, and settling time. The purpose of using the fitness function is to detect the best parameters for the controller to determine the optimal parameters for the FPA-tuned PI controllers used in a doubly fed induction generator (DFIG) system. Some of the most popular and effective error functions taken into consideration in controller design are the Integral of Time multiplied by Absolute Error (ITAE), the Integral of Squared Error (ISE), the Integral of Time multiplied by Squared Error (ITSE), and the Integral of Absolute Error (IAE). The objective function Integral of Time Multiplied Absolute Error (ITAE) is considered for estimating the gain of the controllers proposed. The ITAE reduces the settling time and peaks the overshoot [22]. Equation (31) shows the expression of the ITAE objective function.

$$J = \int_{t1}^{t2} (\lambda 1\ |\ \Delta V| + \lambda 2 |\Delta P| + \lambda 3 |\Delta I_{rc}| + \lambda 4 |\Delta I_{gc}| + \lambda 5 |\Delta V_{dc}|).t.dt \qquad (31)$$

Where;

t_1 and t_2 are the disturbance beginning and end times, respectively ,$\lambda 1$, $\lambda 2$, $\lambda 3$, $\lambda 4$, $\lambda 5$ are the selected weighting factors [22], ΔV is the voltage error when disturbance occurs, ΔP is the power error when disturbance occurs, ΔI_{rc} is the rotor current error when disturbance occurs, ΔI_{gc} is the grid current error when disturbance occurs, ΔV_{dc} is the DC bus voltage error when disturbance occurs.

5. Flower pollination algorithm

5.1. Characteristics of flower pollination

Bio-inspired meta-heuristic algorithms have, over the last few years, played a vital role in the area of optimization. The flower pollination algorithm (FPA), developed by Yang et al. [23] in 2013, is one of several bio-inspired algorithms that have exploited the flower pollination pattern in nature. This algorithm has been used in several applications of hybrid energy conversion systems. Moghaddam et al. [24] investigated the optimal design and energy management of hybrid systems (PWFHS) integrating photovoltaic (PV) panels, a wind turbine (WT), and a fuel cell (FC) based on hydrogen storage (HS) to minimize the total net present cost (TNPC) of northwest region of Iran using the intelligent flower pollination algorithm (FPA) [24]. Generally, about 80% of plants are blossoming species; their reproduction occurs through pollination. Pollination means transfer of pollen from one flower to a similar one or to a different one [25]. The transport of pollen can take place by pollinators such as birds, insects, bats and other animals. Two main types of pollination may be distinguished; the first one is biotic and is done by birds, animals, bats and insects, and the second one is abiotic and happens through wind and diffusion [26]. Moreover, pollination can be of two kinds, i.e. cross-pollination and self-pollination. Cross-pollination occurs when pollen is transferred from the anther of one flower to the stigma of another flower on a different organism of the same variety. However, self-pollination takes place as the pollen from the anther is fixed on the stigma of the same flower, or another flower of the same species. Flower pollination is viewed as the survival of the fittest and the optimal reproduction of a particular plant species. Some insects, and particularly bees, have a Levy flight behaviour with leaps or flight distance steps that follow a Levy distribution. It has been established that, in general, birds and insects take part in the flower pollination process. The process is known as flower constancy. Birds and insects that participate in pollination, jump or fly to certain species of flowering plants only. Moreover, it is interesting to know that flowers provide the food needed by certain birds and insects. The floral constancy enhances the pollination operation in a number of specific flower types and therefore maximizes reproduction. It is worth noting that, in the flower pollination algorithm (FPA), various floral features, namely the flower constancy and pollinator behavior, involved in the pollination process, were idealized based on the following rules [27]:

a) Biotic pollination and cross-pollination are considered global pollination processes whereas pollen-carrying pollinators perform Levy flights.
b) Abiotic pollination and self-pollination are viewed as local pollination processes.

c) Flower constancy is the disposition of individual pollinators to solely visit certain types of morphs within a species, thus bypassing other flower species.

d) Local pollination and global pollination are controlled by a switch probability "p" that belongs to the interval [0, 1]. Note that local pollination can have a significant fraction of "p" in the overall pollination activities due to physical proximity and other factors such as wind.

5.2. Global pollination and local pollination

The flower pollination algorithm (FPA) consists of two fundamental phases, namely the global pollination process and the local pollination process. In the global pollination process, the pollen of flowers is transported by pollinators. Pollinators may sometimes fly and move over quite long distances. Global pollination can be mathematically expressed as follows [28]:

$$x_i^{t+1} = x_i^t + \gamma L(\lambda)(x_i^t - g_*) \tag{32}$$

Where x_i^t corresponds to the solution vector x of pollen *i* at iteration *t*, g_* is the actual best solution of all solutions at the present iteration, and γ is a scaling factor used to control the step size. Also, L(λ) is the Levy flight-based step size that represents the strength of the pollination.

It is worth note that pollinators can move over long distances, but at different step lengths. The Levy flight can be used to mimic the random travelling of pollinators [29]. Taking into consideration a Levy distribution, one could express:

$$L \sim \frac{\lambda\Gamma(\lambda)\sin(\pi\lambda/2)}{\pi}\,\frac{1}{S^{1+\lambda}}\,, (S >> S_0 > 0) \tag{33}$$

Where *Γ(λ)* is the standard gamma function, assuming that the Levy distribution is valid for long steps. Therefore, both rules 2 and 3 for local pollination can actually be expressed as follows:

$$x_i^{t+1} = x_i^t + \varepsilon\,(x_j^t + x_k^t) \tag{34}$$

Where x_j^t and x_k^t are solution vectors for pollen *j* and pollen *k* at iteration *t*, from different flowers of the same plant species. The equation imitates the flower constancy in limited neighborhoods. Assuming that x_i^t and x_k^t are solution vectors for pollen *j* and pollen *k* at iteration *t*, coming from the same species or chosen from the same population, then this would represent a random local walk; a graph can be plotted from a uniform distribution within the interval [0, 1]. The pseudo code of the flower pollination algorithm is given below.

5.3. Pseudo code of the flower pollination algorithm

The flower pollination algorithm based on solar PV parameter estimation was investigated by Alam et al. [20]. Peesapati et al. [31] studied the flower pollination algorithm based on multi-objective congestion management taking into account optimal capacities of distributed generations. Zhang et al. [32] developed a combined model based on the complete empirical mode decomposition adaptive noise (CEEMDAN), which is a modified flower pollination algorithm (FPA) for wind speed forecasting. A number of conventional nonlinear adaptive algorithms were established and proposed for the adaptive control of variable-speed wind turbines [33-36]. They have the capacity to automatically adjust the excitation winding voltage of the wind turbine to the adaptive algorithms in order to regulate the rotor speed tracking process. The above mentioned algorithms have the potential to stabilize the active and reactive output power of the wind turbines when the wind speed changes. According to the related literature, these algorithms generally adapt to ideal operational conditions but the interaction between the grid and the wind turbine is not taken into consideration. A new multivariable control strategy is proposed for variable speed and variable pitch wind turbines [37]. In addition, the use of dynamical variable adaptive structure controllers has been proposed to regulate the active and reactive power which is then injected into the power grid connected to wind energy conversion systems [38].

Table 3 shows the parameter settings for each corresponding optimization algorithm taken into consideration for optimizing the DFIG by tuning the PI controller parameters. The flowchart illustrated in Figure 7 shows the algorithm proposed for tuning the PI controllers.

Table 3. Parameter settings for GA and PFA algorithms.

Parameter settings	
Genetic Algorithm (GA)	**Algorithm flower pollination (FPA)**
Population size = 25 Generation size=50 Roulette wheel Mutation probability=0.01%	Number of flowers =25 Probability switch=0.8

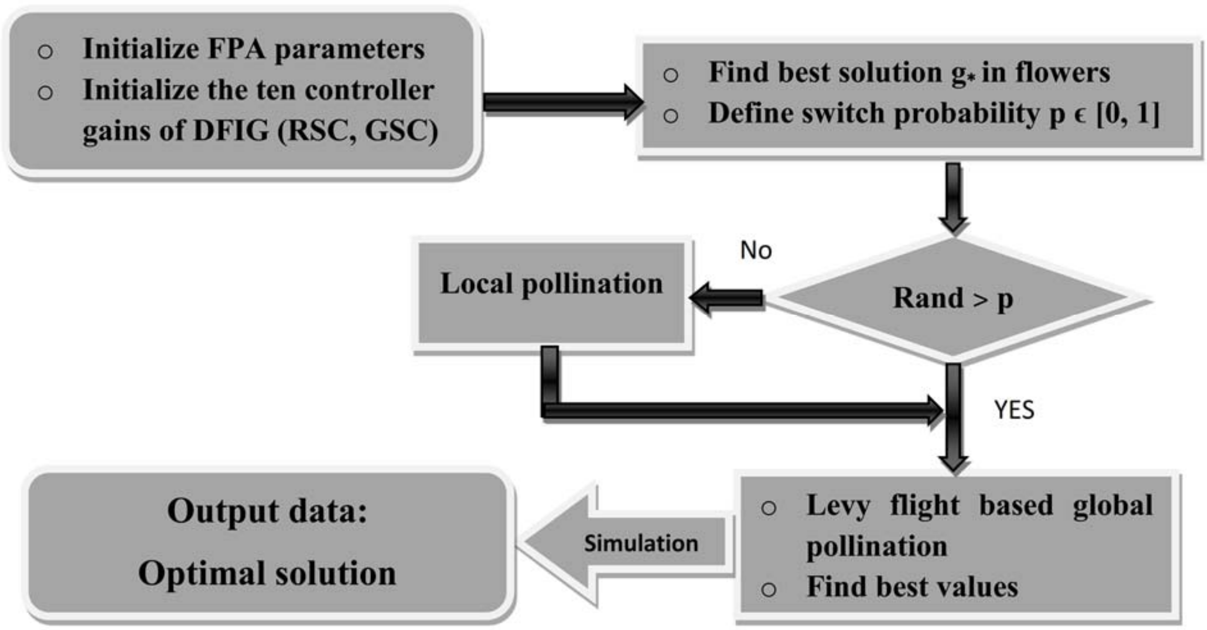

Figure 7. Flower pollination algorithm flowchart.

6. Results and discussion

6.1. Case study without short circuit faults in the network (normal conditions)

The three control techniques give almost the same results in normal operation mode. The simulation results under normal conditions are displayed in Figure 8.

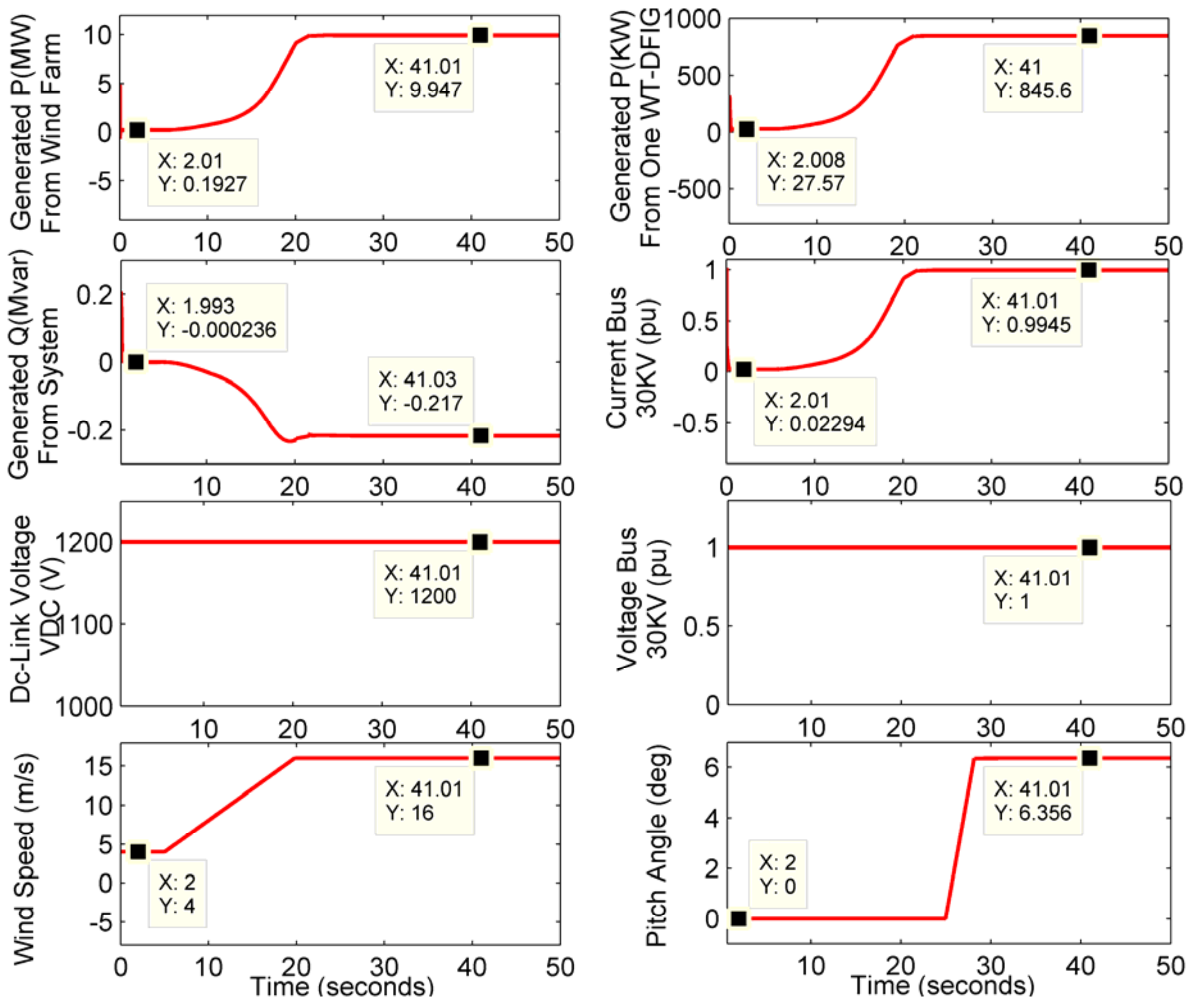

Figure 8. Simulation results for normal operation and parameters set in Table 2, with step changes in wind speed ranging from 4 to 16 m/s at intervals of 50 s.

6.2. Case study of a single-phase short circuit fault on the 30 kV grid line

In this case study, the response of the doubly fed induction generator (DFIG) is analyzed under single-phase short circuit fault conditions on the 30 kV line of the power grid.

In order to validate the flower pollination algorithm illustrated in figure 7, a simulation model developed in Matlab/Simulink environment was tested using three different controllers, namely the PI (initial design), GA-PI and FPA-PI, and under various power and fault conditions, as shown in Tables 3, 4 and 5, respectively. The simulation results revealed that the optimal controller design of a doubly fed induction generator (DFIG) wind turbine, using the flower pollination algorithm (FPA), could be employed to improve the performance of the system at any time a fault or interruption occurs. The response of the optimized doubly fed induction generator (DFIG) was simulated under the operating conditions of a single-phase short circuit fault in the power grid next to the load. The fault started at t= 40 s and lasted for 150 ms. The simulation results indicated that the FPA optimized PI controller gave a better dynamic response in comparison to other controllers (PI controllers used in DFIG initial design as well as the GA optimized PI controllers). The numerical gain values of each PI controller tuning parameter using the different optimization techniques are given in Table 4.

Table 4. Gain values for PI controllers (initial design) and PI controllers tuned by the genetic algorithm and then by FPA-based PI controllers.

Controllers		**Initial design**	**Optimization techniques**	
		PI	**GA-PI**	**FPA-PI**
Voltage AC regulator (RSC)	Kp_v	0.8	1.6035	2.3135
	Ki_v	325	264.6851	395.6529
Power regulator (RSC)	Kp_p	1.2	1.1404	1.9145
	Ki_p	80	184.2629	120.5739
Current regulator (RSC)	Kp_{rc}	0.2	0.8377	0.4848
	Ki_{rc}	9	12.7684	11.8414
Current regulator (GSC)	Kp_{gc}	8	4.9837	2.7557
	Ki_{gc}	250	149.9687	70.7500
Voltage DC regulator (GSC)	Kp_{vdc}	0.0018	0.0130	0.0142
	Ki_{vdc}	0.08	0.4621	0.2000

Figures 9, 10, 11, 12, 13 and 14 illustrate the system performance comparison of responses from PI controllers (initial design) and the new PI controllers obtained from different optimization techniques intended to tune these PI controllers (initial design). Note that the blue line, the green line and the red line represent the system response for the PI initial design controller, GA-based PI controller and the FPA-PI controller proposed, respectively.

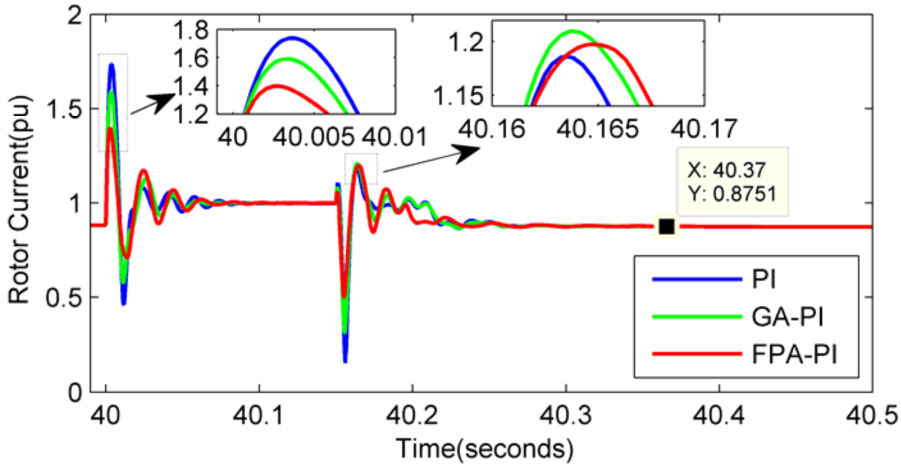

Figure 9. Rotor current response (pu) at parameters set in Table 2.

Figure 9 shows that when using the FPA-PI controller, the rotor current overshoot is lower at the beginning and at the end of the disturbance than when the GA-PI and PI initial design controllers are used. With the FPA-PI controller, the excess current to the rotor circuit is reduced to avoid a power outage or failure and to ensure the continuity of electricity production. The electric network stabilizes quickly after the disruption. At the beginning of the disturbance, the rotor current is 1.737 pu with the initial PI regulator; it is 1.590 pu with the GA-PI regulator and 1.398 pu with the optimal FPA-PI regulator. However, at the end of the disturbance, this rotor current is 1.186 pu with the initial PI regulator, 1.210 pu with the GAPI regulator and 1.198 pu with the optimal FPA-PI regulator. Moreover, stability time is 40.33 s with the PI regulator initial design, 40.33 s with the GA-PI regulator and 40.32 s with the optimal FPA-PI regulator.

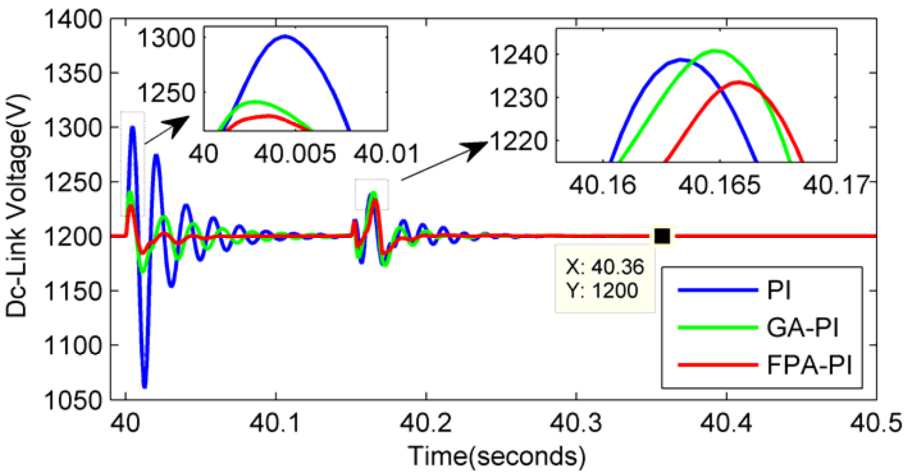

Figure 10. Response of the DC-link voltage at parameters set in Table 2.

Figure 10 indicates that when using the FPA-PI controller, the DC bus over voltage is lower, at the beginning and at the end of the disturbance, than when the PI initial design and GA-PI controllers are used. The DC bus voltage at the beginning of the fault is 1301 V with the PI regulator initial design, while it is 1241 V with the GA-PI regulator and 1228 V with the optimal FPAPI regulator. Similarly, the DC bus voltage at the end of the disturbance is 1239V with the PI regulator initial design, 1241 V with the GA-PI controller, and 1228 V with the optimal FPAPI regulator. Furthermore, the DC bus voltage response time at the end of the disturbance is 40.28 s with the PI regulator initial design, 40.27 s with the GA-PI regulator and 40.22 s with the optimal FPA-PI regulator. It is also worth noting that using the optimal design of the DFIG with the FPA-PI controller the voltage stability time of the continuous bus can be reduced when disturbance occurs. In addition, the FPA-PI controller reduces the DC bus over-voltage in the case of a short-circuit failure.

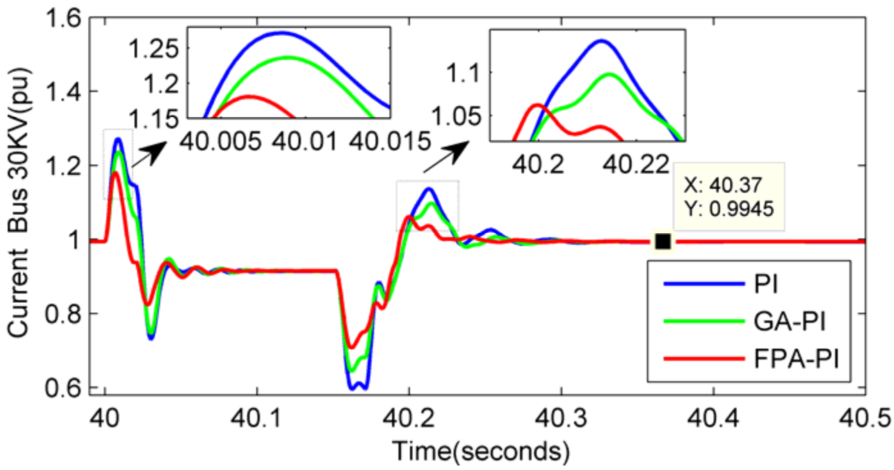

Figure 11. Current response at bus 30 kV (pu) at parameters set in Table 2.

Figure 11 displays the simulation results in the case of a 30 kV current bus. One can clearly note that, when using the FPA-PI controller, 30 kV current bus overflow is lower at the beginning and at the end of the disturbance, than when using the GA-PI and PI initial design controllers. The FPAPI controller reduces the 30 kV current bus overflow and stability time at the end of disturbance. The rotor current at the beginning of the disturbance is 1.272 pu with the initial PI regulator; while it is 1.237 pu with the GA-PI regulator and 0.181 pu with the optimal FPA-PI regulator. The 30 kV current bus (the current on bus voltage 30 kV) at the end of the disturbance is 1.137 pu with the initial PI regulator, 1.098 pu with the GA-PI regulator and 1.062 pu with the optimal FPA-PI regulator. Stability time is 40.32s with the PI regulator initial design, 40.32 s with the GA-PI regulator and 40.28 s with the optimal FPA-PI regulator and 40.27 s with the optimal FPA-PI regulator.

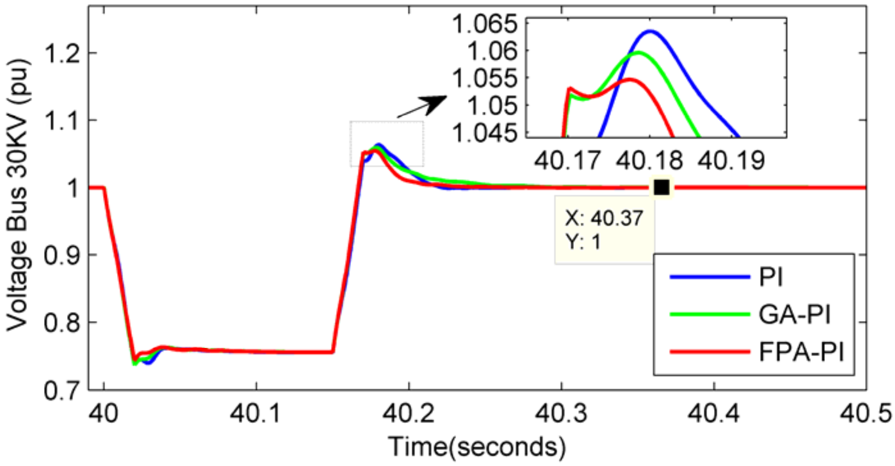

Figure 12. Voltage response at bus 30KV (pu) at parameters set in Table 2.

The simulation results of the bus voltage at 30 kV are displayed in Figure 12. It is observed that, when using the controller FPA-PI, the excess of voltage at bus 30 kV is lower, at the end of the disturbance, than when using the GA-PI controller and PI initial design controller. The FPA-PI controller reduces the overflow of bus voltage 30 kV and the stability time at the end of disturbance. The bus voltage at 30 kV at the end of the disturbance is 1.064 pu with the initial PI regulator, 1.061 pu with the GA-PI regulator and 1.055 pu with the optimal FPA-PI regulator. Similarly, the stability time is equal to 40.27s with the PI regulator initial design, 40.27 s with the GA-PI regulator and 40.26 s with the optimal FPA-PI regulator. It is worthy of note that the FPA-PI controllers present the fastest time after perturbation. In the present case, the results given by the GA-based PI controllers are very close to those obtained by the FPA controllers.

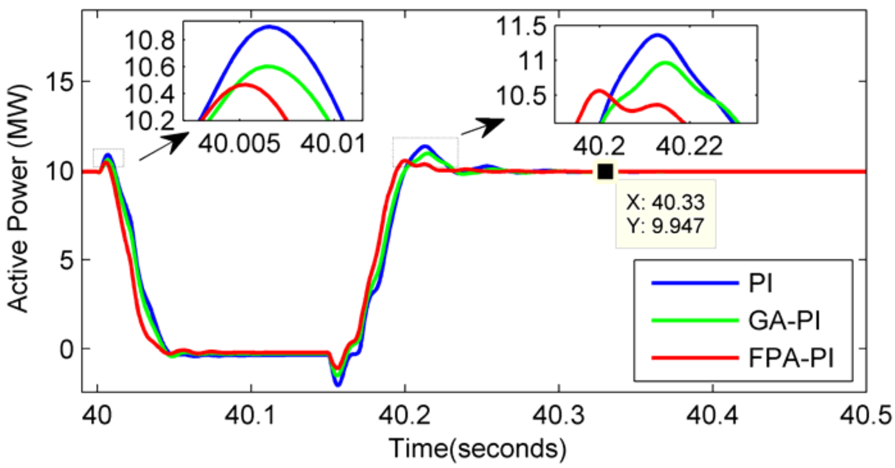

Figure 13. Response of active power (MW) at parameters set in Table 2.

Figure 13 shows the simulation results of the active power. It is noted that, when using the FPA-PI controller, the excess active power is lower at the beginning and at the end of the disturbance, than when the GA-PI controller and PI initial design controller are used. The FPA-PI controller reduces the active power overrun and the stability time at the end of disturbances. The active power at the beginning of the fault is 10.900 MW with the initial PI regulator; it is 10.600 MW with the GA-PI regulator and 10.470 MW with the optimal FPA-PI regulator. The active power at the end of the disturbance is 11.360 MW with the initial PI regulator, 10.940 MW with the GA-PI controller and 10.560 MW with the optimal FPA-PI regulator. As for the stability time, it is 40.24s with the PI initial design regulator, 40.24 s with the GA-PI regulator and 40.22 with the FPA-PI regulator.

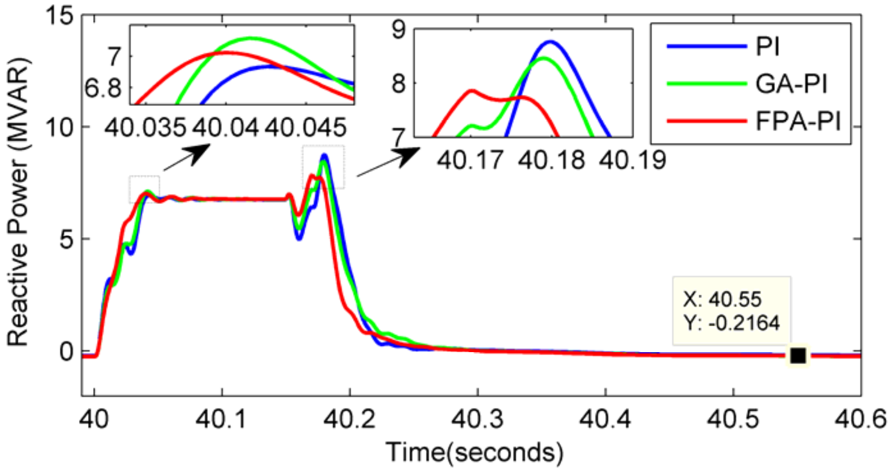

Figure 14. Variation of the reactive power (Mvar) as a function of time, at parameters set in Table 2.

The simulation results of the reactive power illustrated in Figure 14 indicate that the excess reactive power obtained with the FPA-PI controller is lower, at the beginning and at the end of the disturbance, than that of the GA-PI and PI initial design controllers. The FPAPI controller reduces the active power overrun and stability time at the end of the disturbance. The reactive power at the beginning of the fault is 6.933 Mvar with the initial PI regulator, 7.115 Mvar with the GA-PI controller and 7.022 Mvar with the FPA-PI regulator. The reactive power at the end of the disturbance is 8.760 Mvar with the initial PI regulator, 8.457 Mvar with the GA-PI controller and 7.857 Mvar with the optimal FPA-PI regulator. Also, the stability time is 40.61s with the PI.

Table 5. Calculated overshoot and settling time.

Response	Technique	Parameter		
		Overshoot at beginning of fault	Overshoot at end of fault	Settling Time at end of fault
Rotor current (pu)	PI	1.737	**1.186**	40.33
	GA-PI	1.590	1.210	40.33
	FPA-PI	**1.398**	1.198	**40.32**
DC-link voltage (V)	PI	1301	1239	40.28
	GA-PI	1241	1241	40.27
	FPA-PI	**1228**	**1234**	**40.22**
Current on Bus 30 kV (pu)	PI	1.272	1.137	40.32
	GA-PI	1.237	1.098	40.32
	FPA-PI	**1.181**	**1.062**	**40.28**
Voltages on Bus voltage 30 kV (pu)	PI	0	1.064	40.27
	GA-PI	0	1.061	40.27
	FPA-PI	0	**1.055**	**40.26**
Active power (MW)	PI	10.900	11.360	40.24
	GA-PI	10.600	10.940	40.24
	FPA-PI	**10.470**	**10.560**	**40.22**
Reactive power (MVAR)	PI	**6.933**	8.760	40.61
	GA-PI	7.115	8.457	40.60
	FPA-PI	7.022	**7.857**	**40.47**

The simulation results indicate that the optimized FPA-PI controller presents a better performance in comparison to the other controllers; indeed, the system proposed results in smaller overshoots and a quicker response to any perturbation. Moreover, it returns to the steady state quickly and presents smaller oscillations. The above figures clearly show the importance of the new GA-based PI controller in terms of high settling time with minimum damping oscillations and peak overshoot. The numerical values of each response from the algorithm optimized controller are given in Table 5, together with a detailed summary of the simulation results.

Conclusions

This study is focused on a new application of Proportional Integral (PI) controllers that uses the flower pollination algorithm (FPA) to improve the performance of a doubly fed induction generator (DFIG). The dynamic response performance of the FPA-based PI controller proposed is compared with the responses of the PI controller (initial design) on the DFIG and the GA optimized PI controller. In addition, the cumulative performance of the system clearly indicates that the algorithm proposed guarantees the best dynamic control response in terms of minimum settling time and minimum peak overshoot should a short-circuit failure occurs on the power grid. Furthermore, this study demonstrates that the flower pollination algorithm (FPA)-based PI controller proposed guarantees a faster response speed when compared to that of a PI controller and GA-based PI controller. The quality of the electricity supply during a disturbance is much better. However, with regard to the GA-based PI performance, sometimes the peak overshoots in the PI controller-based system proposed are higher than those generated by the PI controller of a DFIG. The results of the simulation carried out with the GA-PI controller lead us to the conclusion that the overruns and response time are smaller in comparison to those obtained with the PI controllers. However, the FPA-based PI controller develops even smaller overruns throughout the transition phase (short-circuit fault) with earlier responses and a shorter response time compared to those obtained with PI initial design controllers and GA-based PI controllers. These findings suggest that the FPA-PI controller performance is better during the transition phase in comparison to that of the PI controller and the GA-PI controller.

REFERENCE

[1] L. Zhenya. Innovation in Global Energy Interconnection Technologies. Global Energy Interconnection, Chapter 6, pp. 239-272, ISBN: 978-0-12-804405-6, 2015.

[2] H. Mahvash, S.A. Taher, M. Rahimi, M. Shahidehpour. Enhancement of DFIG performance at high wind speed using fractional order PI controller in pitch compensation loop. International Journal of Electrical Power and Energy Systems, vol. 104, pp. 259-268, 2019.

[3] S. Makhloufi, A. Mekhaldi, M. Teguar. Three powerful nature-inspired algorithms to optimize power flow in Algeria's Adrar power system. Energy, vol. 116, pp.1117-1130, 2016.

[4] A. Ahmed, M.M.H. Galib, S.M.K. Zaman, G. Sarowar. An optimization methodology of susceptance variation using lead-lag controller for grid connected FSIG based wind generator system. Journal of the Franklin Institute, vol. 355 (1), pp.197-217, 2018.

[5] Z. Qu, K. Zhang, W. Mao, J. Wang, C. Liu, W. Zhang. Research and application of ensemble forecasting based on a novel multi objective optimization algorithm for wind-speed forecasting. Energy Conversion and Management, vol. 154, pp. 440–454, 2017.

[6] A.Y. Abdelaziz, E.S. Ali, S.M. Abd Elazim. Implementation of flower pollination algorithm for solving economic load dispatch and combined economic emission dispatch problems in power systems. Energy, vol. 101, pp.506-518, 2016.

[7] J. Dai, D. Liu, Y. Hu, X. Shen. Research on Joint Power and Loads Control for Large Scale Directly Driven Wind Turbines. Journal of Solar Energy Engineering, vol. 136 (2): 021015, 2014.

[8] Adel A.A. Elgammal. Optimal Design of PID Controller for Doubly-Fed Induction Generator-Based Wave Energy Conversion System Using Multi Objective Particle Swarm Optimization. Journal of Technology Innovations in Renewable Energy, vol. 3 (1), pp.21-30, 2014.

[9] H.M. Hasanien, G.M. Hashem. A cuckoo search algorithm optimizer for steady-state analysis of self-excited induction generator. Ain Shams Engineering Journal, vol. 9 (4), pp. 2549-2555, 2018.

[10] K. Naidu, H. Mokhlis, A.H.A. Bakar, V. Terzija. Performance investigation of ABC algorithm in multi-area power system with multiple interconnected generators. Applied Soft Computing Journal, vol. 57, pp. 436-451, 2017.

[11] H. Suryoatmojo, A.M.B. Zakariya, S. Anam, A. Musthofa, I. Robandi. Optimal Controller for Doubly Fed Induction Generator (DFIG) Using Differential Evolutionary Algorithm (DE). International Seminar on Intelligent Technology and Its Applications (ISITIA), DOI: 10.1109/ISITIA.2015.7219972, 2015.

[12] X.S. Yang, Z. Cui, R. Xiao, A.H. Gandomi, M. Karamanoglu. Swarm Intelligence and Bio-Inspired Computation: Theory and Applications. Elsevier Insights, ISBN: 978-0-12-405163-8, 2013.

[13] K. Jagatheesan, B. Anand, S. Samanta, N. Dey, V. Santhi, A.S. Ashour, V.E. Balas. Application of flower pollination algorithm in load frequency control of multi-area interconnected power system with nonlinearity. Neural Computing and Applications, vol. 28 (1), pp. 475–488, 2017.

[14] I. Hussain, S. Ranjan, D.C. Das, N. Sinha. Performance Analysis of Flower Pollination Algorithm Optimized PID Controller for Wind-PVSMES-BESS-Diesel Autonomous Hybrid Power System. International Journal of Renewable Energy Research-IJRER, vol. 7 (2), pp. 643-651, 2017.

[15] Hanan M. Askaria, M.A. Eldessouki, M.A. Mostaf. Optimal Power Control for Distributed DFIG Based WECS Using Genetic Algorithm Technique. American Journal of Renewable and Sustainable Energy, vol. 1(3), pp.115-127, 2015.

[16] A. Zemmit, S. Messalti, A. Harrag. A new improved DTC of doubly fed induction machine using GA-based PI controller. Ain Shams Engineering Journal, vol. 9 (4), pp.1877-1885, 2018.

[17] E. Mohammadi, R. Fadaeinedjad, G. Moschopoulos. An electromechanical emulation-based study on the behaviour of wind energy conversion systems during short circuit faults. Energy Conversion and Management, vol. 205 (1), Article 112401, 2020.

[18] D.W. Gao, X. Wang, J. Wang, T. Gao, M. Stefanovic, X. Li. Optimal Pitch Control Design With Disturbance Rejection for the Controls Advanced Research Turbine. Journal of Solar Energy Engineering, vol. 141 (1): 011005, 2019.

[19] B. Shen, B. Mwinviwiwa, Y. Zhang, and B. T. Ooi. Sensorless maximum power point tracking of wind by DFIG using rotor position phase lock loop (PLL). IEEE Trans. Power Electronic, vol. 24(4), pp. 942–951, Apr. 2009.

[20] Y. Zou, M. Elbuluk, and Y. Sozer. A novel maximum power points tracking (MPPT) operation of doubly-fed induction generator (DFIG) wind power system. IEEE Industry Application. Soc. Annual Meeting (IAS), pp. 1–6, 2012.

[21] A.D. Falehi. Optimal Power Tracking of DFIG-Based Wind Turbine Using MOGWO-Based Fractional-Order Sliding Mode Controller. Journal of Solar Energy Engineering, vol. 142 (3): 031004, 2020.

[22] E. Celik, N. Ozturk. First application of symbiotic organisms search algorithm to off-line optimization of PI parameters for DSP-based DC motor drives. Neural Computing and Applications vol.30 (5), pp. 1699-1699, 2018.

[23] P.C. Nayak, U.C. Prusty, P.C. Sahu, R.C. Prusty. Design and Tuning of Flower pollination algorithm based 2DOF controller in AGC of multi area thermal wind system. International Journal of Advanced Research in Electronics and Communication Engineering (IJARECE), vol. 7 (2), pp. 118-126, 2018.

[24] M. Moghaddam, A. Kalam, S.A. Nowdeh, A. Ahmadi, M. Babanezhad, S. Saha. Optimal sizing and energy management of stand-alone hybrid photovoltaic/wind system based on hydrogen storage considering LOEE and LOLE reliability indices using flower pollination algorithm. Renewable Energy, vol. 135, pp. 1412-1434, 2019.

[25] T. Kathuria, A. Gupta, J. Kumar, V. Kumar, K.P.S. Rana. Study of optimization methods for tuning of PID gains for three link manipulator. Proceedings of the 7th International Conference Confluence 2017 on Cloud Computing, Data Science and Engineering, Article number 7943131, pp. 99-104, 2017.

[26] T. Wiangtong, J. Sirapatcharangkul. PID Design Optimization Using Flower Pollination Algorithm for a Buck Converter. 17th International Symposium on Communications and Information Technologies, ISCIT 2017, pp. 1-4, 2018.

[27] O.P. Bharti, R.K. Saket, S.K. Nagar. Controller Design of DFIG Based Wind Turbine by Using Evolutionary Soft Computational Techniques. Engineering, Technology & Applied Science Research, vol. 7 (3), pp. 1732-1736, 2017.

[28] M. Abd-Elkareem, E. Abd-Elalim, M.A. Ebrahim. Optimal Controllers for DFIG based Wind Farm connected to Grid using Evolutionary Techniques. International Journal of New Technologies in Science and Engineering, vol. 2 (5), pp. 87-96, 2015.

[29] D. Lakshmi, A. Fathima, R. Muthu. A Novel Flower Pollination Algorithm to Solve Load Frequency Control for a Hydro-Thermal Deregulated Power System. Circuits and Systems, vol. 7, pp.166-178, 2016.

[30] D.F. Alam, D.A. Yousri, M. Eteiba. Flower Pollination Algorithm based solar PV parameter estimation. Energy Conversion and Management, vol. 101, pp. 410-422, 2015.

[31] R. Peesapati, V.K. Yadav, N. Kumar. Flower pollination algorithm based multi-objective congestion management considering optimal capacities of distributed generations. Energy, vol. 147, pp. 980-994, 2018.

[32] W. Zhang, Z. Qu, K. Zhang, W. Mao, X. Fan. A combined model based on CEEMDAN and modified flower pollination algorithm for wind speed forecasting. Energy Conversion and Management, vol. 136, pp.439-451, 2017.

[33] Y. Liu, Z. Wang, L. Xiong, J. Wang, S. Liu. DFIG wind turbine sliding mode control with exponential reaching law under variable wind speed. International Journal of Electrical Power and Energy Systems, vol. 96, pp. 253-260, 2018.

[34] Y.D. Song, B. Dhinakaran, X.Y. Bao. Variable speed control of wind turbines using nonlinear and adaptive algorithms. Journal of Wind Engineering and Industrial Aerodynamics, vol. 85 (3), pp. 293-308, 2000.

[35] B. Boukhezzar, H. Siguerdidjane. Nonlinear control of variable speed wind turbines for power regulation. Proceedings of IEEE Conference on Control Applications, CCA, 2005.

[36] E. Billy Muhando, T. Senjyu, N. Urasaki, A. Yona, H. Kinjo, T. Funabashi. Gain scheduling control of variable speed WTG under widely varying turbulence loading. Renewable Energy, vol. 32 (14), pp. 2407-2423, 2007.

[37] B. Boukhezzar, L. Lupu, H. Siguerdidjane, M. Hand. Multivariable control strategy for variable speed, variable pitch wind turbine. Renewable Energy, vol. 32, pp. 1273-1287, 2007.

[38] H. De Battista, R. Mantz. Dynamical variable structure controller for power regulation of wind energy conversion systems. IEEE Transactions on Energy Conversion, vol. 19 (4), pp.756-763, 2004.

List of figures

List of tables